

AES 770 Satellite Remote Sensing II

Aerosol Optical Depth Retrieval

Mitchell Dodson

October 17, 2023

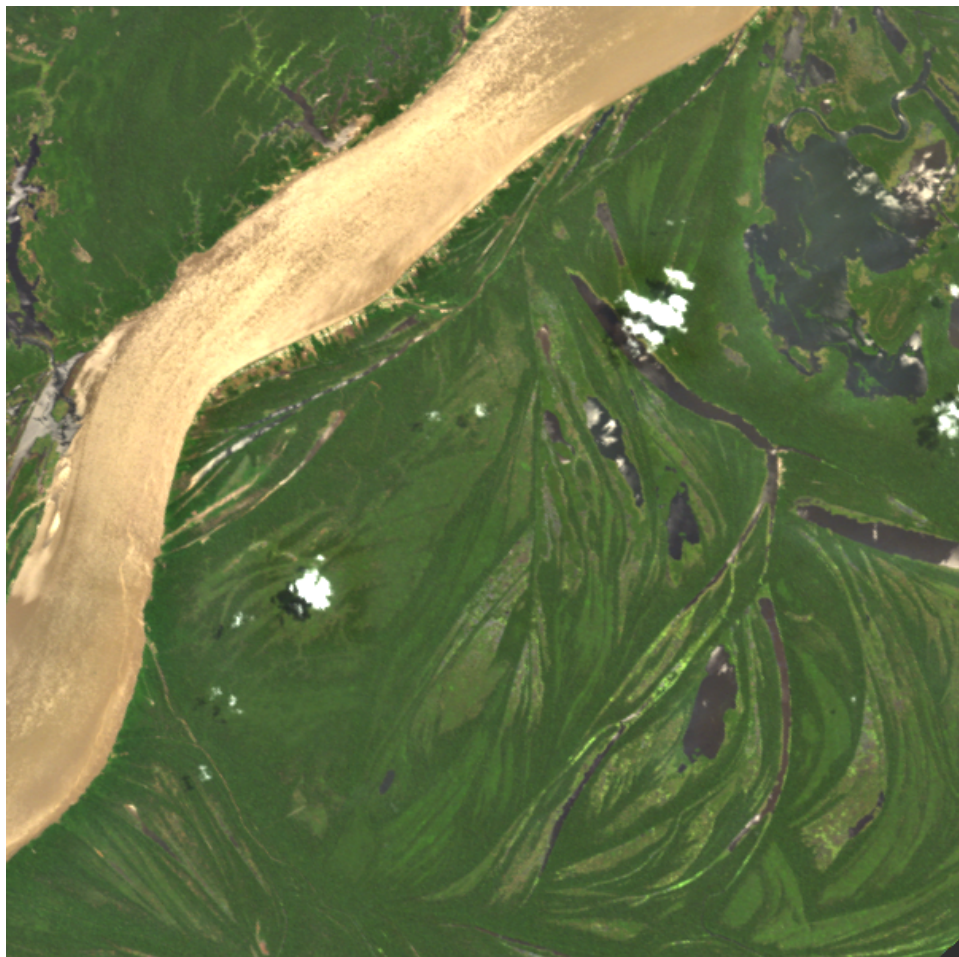


Figure 1: Truecolor over the Amazon, captured by DESIS on 09/03/2020 at 1446z

1 Abstract

Aerosols are a critical part of Earth's climate system since they directly impact Earth's energy budget by scattering and absorption, indirectly impact cloud properties by serving as condensation nuclei, and have a measurable impact on human health. Aerosol retrievals from satellite data are important for understanding the behavior of aerosols because they offer a broad view of the spatial distribution and movement of aerosol plumes, as opposed to higher-confidence but discrete data from ground-based photometers. In this report,

I outline my implementation of an aerosol optical depth (AOD) retrieval algorithm over land using the DESIS hyperspectral radiometer, and focusing on imagery containing rural aerosol types over the Amazon Rainforest. The retrieval strategy tiles the field of regard into 10x10 pixels, and uses the unique spectral response curve of any dark vegetation within a tile to estimate the surface reflectance in the $.64\mu\text{m}$ (RED) channel based on $.82 - .88\mu\text{m}$ (NIR).

2 Theoretical Basis

$$\rho^{*,M}(\lambda, \theta, \theta_0, \phi) = \rho_a^M(\lambda, \theta, \theta_0, \phi) + \frac{F_s^{\downarrow,M}(\lambda, \theta_0)T(\lambda, \theta)\rho(\lambda, \theta, \theta_0, \phi)}{1 - s^M(\lambda)\rho'(\lambda)} \quad (1)$$

$$\frac{dN(r)}{dr} = \sum_{i=1}^2 \left(\frac{N_i}{\ln(10) r \sigma_i \sqrt{2\pi}} \exp \left[-\frac{\log(r) - \log(r_i)}{2\sigma_i^2} \right] \right) \quad (2)$$

$$\rho^* = \nu \rho_f^* + (1 - \nu) \rho_c^* \quad (3)$$

Although aerosols have a wide variety of size profiles and scattering properties, they can be broadly categorized into fine and coarse modes corresponding to effective radii around $0.05 - 1\mu\text{m}$ or greater than $2\mu\text{m}$, respectively [1][2]. Fine modes represent materials like urban pollution and smoke, while coarse mode particles include dust and organic debris, pollen, and soot.

Since the fine mode particles have radii around the visible and near-infrared spectrum, they dominantly affect incident light by Mie scattering. Aerosol phase functions are generally considerably anisotropic, which makes their effect on observed radiance quite sensitive to the viewing geometry. The overall effect of most aerosols is to increase the albedo of the atmospheric column in the solar spectrum, however carbonaceous aerosol types (such as those produced by biomass burning) also absorb an increment of incident light, which warms the surrounding atmospheric layer.

Equation 1 provides a generalized expression for the top-of-atmosphere reflectance ρ^* given a single aerosol mode M , and an unknown aerosol loading. M represents size r_g , phase function P , and single-scatter albedo ω_0 of a constituent type. ρ_a is the atmospheric path radiance given the single-scatter assumption, F_s^{\downarrow} is the direct downward flux incident on the surface, T is the upward transmittance of the atmosphere, s is the ratio of upward radiation that is back-scattered by the atmosphere, ρ is the actual surface reflectance, and finally ρ' is the spherical albedo of the surface below. The first term in the equation is the aerosol path radiance at a particular wavelength λ , which is the quantity most directly related to AOD, and the second term accounts for atmospheric transmittance as well as secondary scattering from the atmosphere back to the surface.

In order to model the effect of multiple distinct aerosol species in the atmospheric column, the aerosol radius distribution with respect to cumulative number count of aerosols are described in terms of a sum over log-normal distributions representing each type, as expressed by Equation 2. It is usually sufficient to express the combined effect of aerosols in terms of the juxtaposition of one coarse and one fine mode based on a-priori knowledge of the season and region of the field of regard [2]. The consequent top-of-atmosphere reflectance is represented by a percentage ν of the reflectance contribution with fine aerosols to the total observed reflectance.

For the purposes of this project, I used the aerosol profiles identified by (Shettle, 1976) [3], which include empirical values for the combined effects of coarse and fine modes for

species typical to rural, urban, oceanic, and general tropospheric regions. These configurations are all included as presets in the SBDART radiative transfer model. Furthermore, since the model accounts for multiple scattering, the second term is implicitly included in the lookup tables I generated with the algorithm.

3 Lookup Table Generation

Parameter	Value	Justification
PHI; NPHI	[0,180]; 8	22.5° even increments of relative azimuth angles.
UZEN; NZEN	[0,85]; 20	4.25° even increments of viewing zenith angles.
SZA	[0,80]; 16	5° even increments of solar zenith angle.
WL	[.4,.1.0]; 120	5 nm even increments of wavelength.
TBAER	[0,20]; 12	Logarithmically spaced increments of aerosol optical depth.
IAER	1, 2, 3, 4	Regional aerosol mode (rural, urban, oceanic, tropospheric)
PBAR	0	No atmospheric scattering or pressure effects
IDATM	1,2	Mid-latitude Summer and tropical atmospheric water vapor profiles, depending on the field of regard.
ISALB	6	Dark vegetated surface
CORINT	True	Correct error in the ΔM scale of the phase function.
IOUT	5	Generate spectral radiance, as well as path-integrated spectral fluxes at the top-of-atmosphere and surface.

Table 1: Outline of the SBDART parameters used for the generation of lookup tables, which include tables for TOA spectral radiance and path-integrated solar irradiance.

Table 1 shows the SBDART configuration I used to generate the lookup tables for AOD retrieval over vegetated surfaces. The subsequent spectral radiance lookup table has 6 orthogonal axes corresponding to the increments in solar zenith angle, AOD, aerosol mode, viewing zenith angle, path-relative azimuth angle, and wavelength. Because of the nonspherical phase functions of many aerosols, it's important that the CORINT parameter is set to True in order to correct for assumptions made in the truncation of the phase function by the DISORT backend used in SBDART [4]. Additionally, SBDART atmospheric correction is turned off because the L2 DESIS product I'm using for analysis is already corrected for the atmosphere and terrain.

4 Retrieval Methodology

4.1 Model Analysis

Figure 2 shows the spectral reflectance factor and anomaly of typical rural aerosol amounts over vegetation (using the response curve included with SBDART). The reflectance is small but slightly stratified in the RED waveband 640 nm, which is the phenomenon typically exploited by comparison to the reflectance in a short-wave infrared (SWIR) channel like 2.24 μm or 3.9 μm . SWIR channels have effective radii that are large enough

not to be strongly attenuated by fine-particle Mie scattering, so they serve as a good baseline for estimating the actual surface reflectance in the RED channel using an empirical ratio.

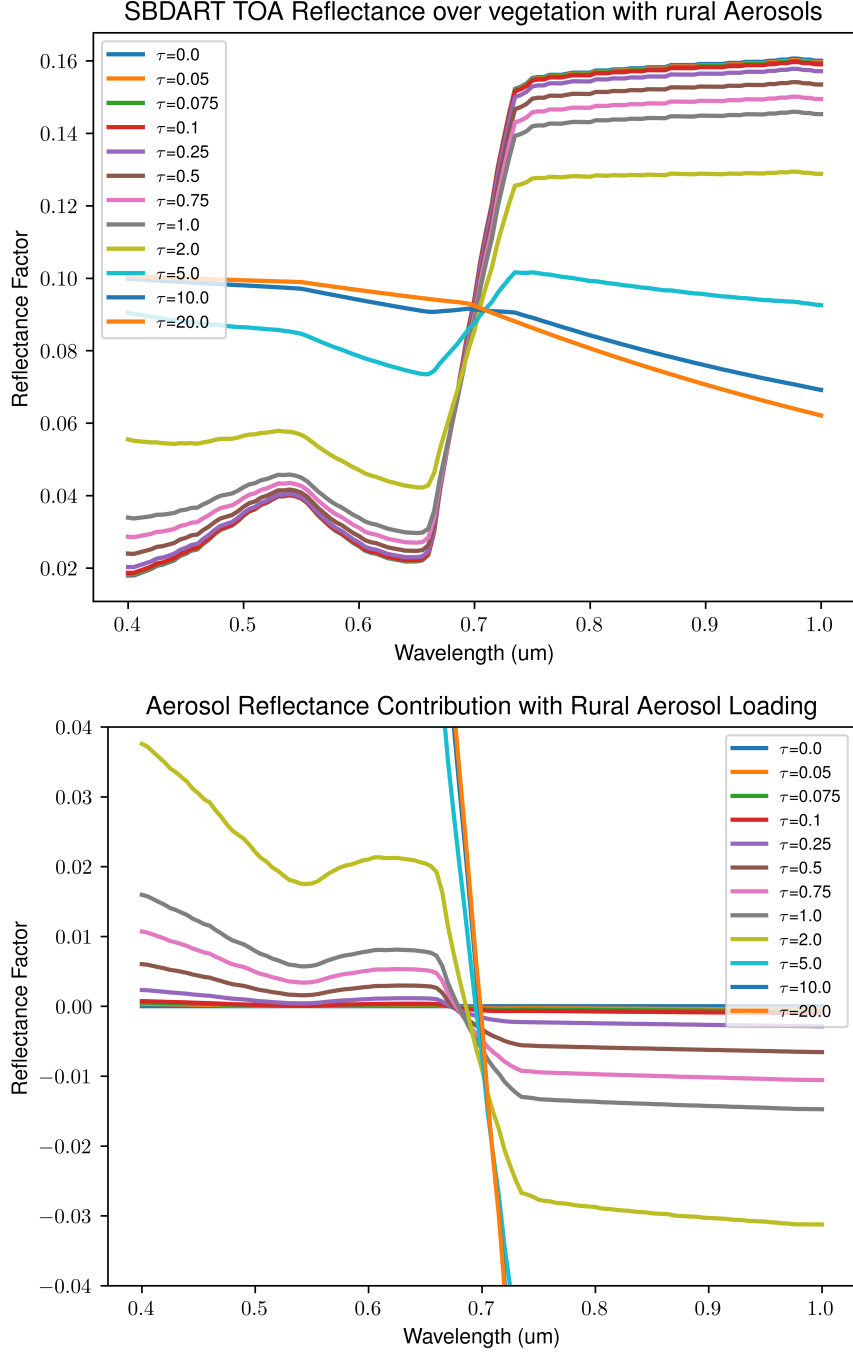


Figure 2: Model-derived spectral response curves over vegetation given multiple rural aerosol loadings, with AOD units given in green channel $\tau(550\text{nm})$. The top plot shows the estimated TOA reflectance (after atmospheric correction), and the bottom plot shows the component of reflectance attributable to aerosol effects. The latter was obtained by subtracting the spectral response of only vegetation ($\tau = 0$) from the aerosol-laden reflectance at each wavelength and aerosol amount.

The aerosol model in Figure 2 corresponds mainly to fine-grained natural materials such as sulfates and organic compounds, but includes a component for continental dust which accounts for about 30% of the total by count. Furthermore, the model has a complex index of refraction, with absorptivity that depends intrinsically on the aerosol loading of the column [5]. According to (Shettle, 1976), the absorptivity peaks in the near-infrared range, hence the decrease in reflectance as wavelength increases [3].

4.2 Dense, Dark Difficulties

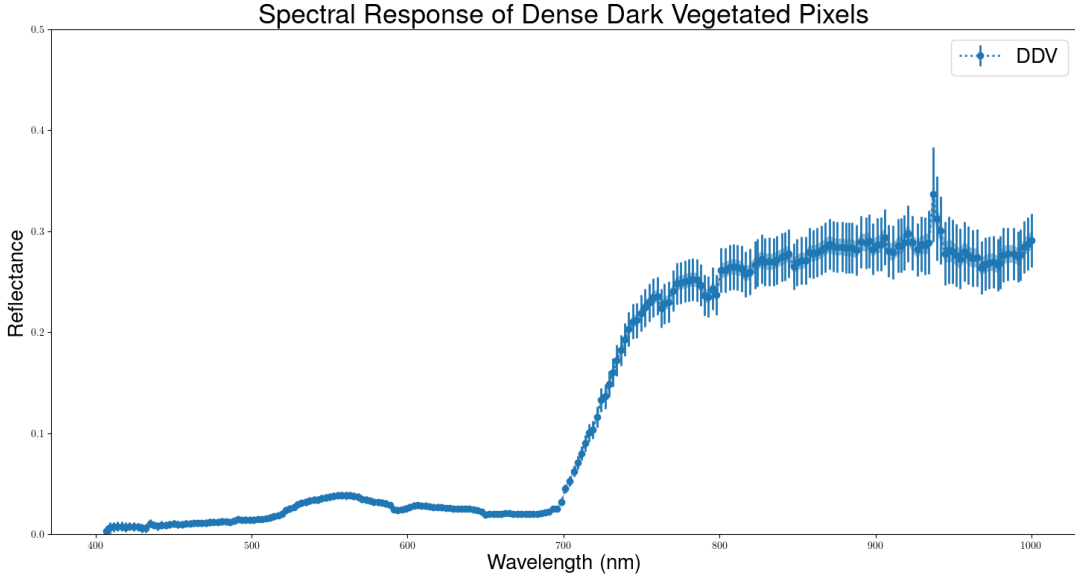


Figure 3: Spectral response of pixels selected as dense dark vegetation.

My procedure for estimating aerosol optical depth is similar to the one used for over-land retrievals by the MODIS operational product, initially outlined by (Kaufman and Tanre, 1997) [5][6]. Since aerosols tend to have concentrations that vary on relatively large spatial scales, the strategy starts by tiling the field of regard into square sub-sections of 10x10 or 20x20 pixels. AOD is retrieved independently for each grouping of pixels by identifying pixels containing dense dark vegetation (DDV) on the surface, and leveraging the characteristic increase in reflectance of vegetation from the visible to near infrared range.

Figure 2 eludes to one of the primary difficulties I encountered while developing the procedure. Since DESIS only includes bands in the $.4 - 1 \mu\text{m}$ range, the above technique for estimating surface reflectance as a ratio of the reflectance in a $2.24 \mu\text{m}$ or $3.9 \mu\text{m}$ cannot be used. Instead, the entire range of the instrument's spectral sensitivity is affected by rural aerosols.

Since typical background continental aerosol optical depth values around $\tau = .3$ are only responsible for a change few thousandths of a reflectance unit, the retrieved AOD is incredibly dependent on the selected surface reflectance. I attempted many strategies for rectifying the additional uncertainty in surface reflectance of vegetated pixels including (1) modifying the lookup table to search for the difference between NIR and RED reflectance

rather than their magnitudes, (2) establishing an a-priori guess for aerosol optical depth based on the ratio of NIR to RED, and (3) using the lookup table to calculate an empirical ratio between RED and the $.7\mu\text{m}$ channel (where the AOD curves intersect).

The first two strategies were unsuccessful because it was difficult to find initial thresholds for DDV pixels that generalized across an entire scene, much less across multiple granules, and the third failed because the rapid increase in vegetation reflectance makes the observed value very sensitive to an increment change in wavelength, and the increase in DESIS-observed reflectance over vegetation is actually near $.73\mu\text{m}$ rather than $.7\mu\text{m}$ as suggested by the model. Attempts to constrain DDV pixels to those with an in-range reflectance jump inevitably made DDV pixel selections too sparse.

4.3 Reference Pixel Selection

$$\frac{NIR}{RED} \geq 4 \text{ and } 0.1 \leq NIR \leq .28 \text{ and } NDVI > .6 \text{ and } RED \leq .04 \text{ and } NDWI < -.6$$
(4)

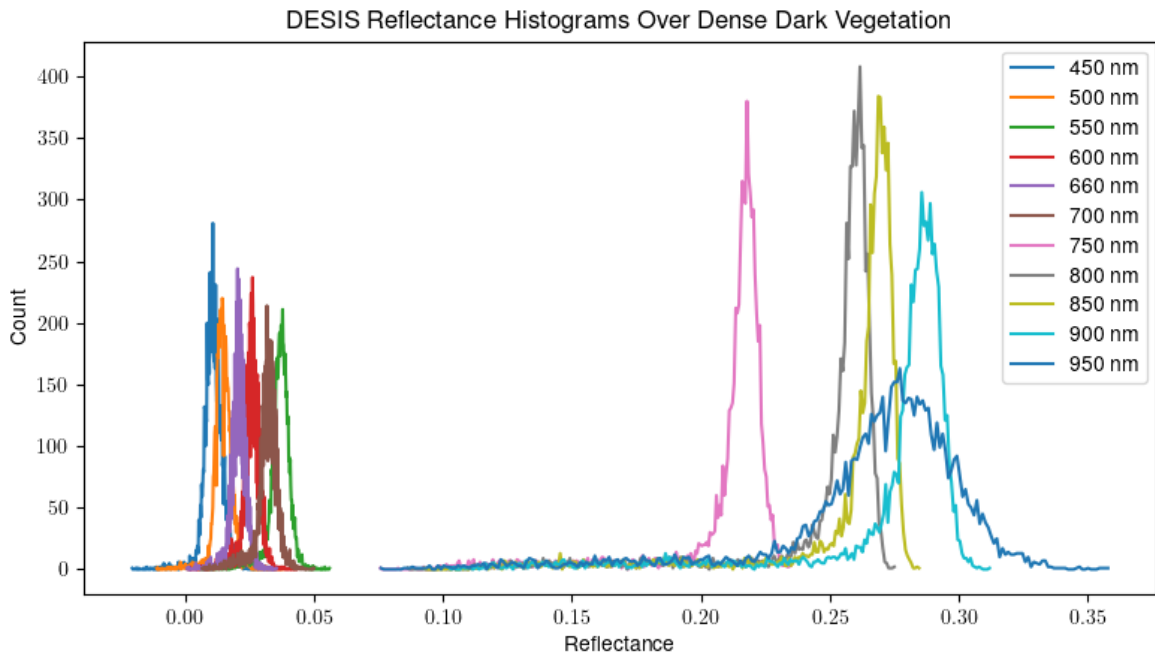


Figure 4: Histograms of DDV pixels in several wavebands. Only the $.55\mu\text{m}$, $.65\mu\text{m}$, and $.85\mu\text{m}$ channels were used for thresholding.

Ultimately, I settled on a method similar to (Richter, 1996) which starts with a moderate a-priori assumption that the background visibility is 23 km, or about $\tau = .27$. The AOD is then used alongside the LUT to approximate the surface reflectance of all pixels identified as vegetation. The algorithm then iteratively changes the upper bound on $.65\mu\text{m}$ surface reflectance until the number of DDV pixels in a tile is within a percentage range of the total number of pixels in the tile [7]. The percentage threshold is set as a hyperparameter, but a threshold of 8% tends to return sufficiently many and sufficiently dark pixels. A more detailed description of my modified version of the procedure follows.

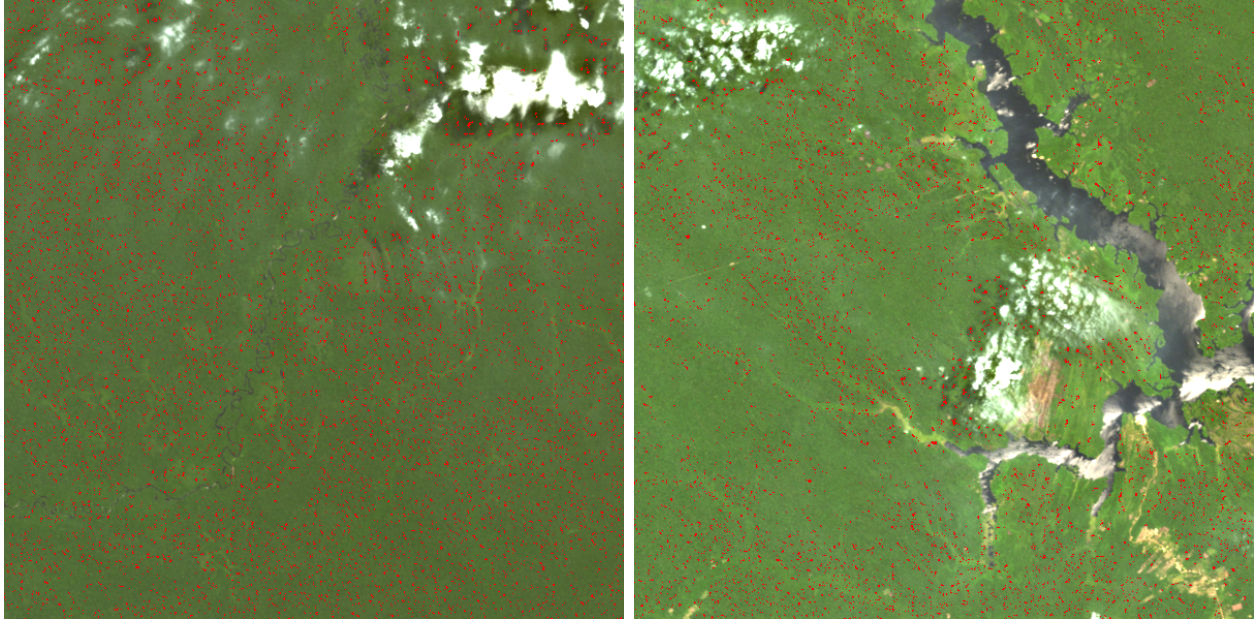


Figure 5: Truecolor RGBs with all DDV pixels selected by my procedure marked in red. There are still some cloud shadow pixels chosen as DDV, which is certainly a source of error, however most of these are later rejected during the AOD inversion for having apparent RED surface reflectances that are outside of the lookup table range.

1. Check whether any pixels in the tile have a NDWI value greater than $-.6$. If so, reject the entire tile, as the reflectance of coastline pixels can sometimes resemble the vegetation spectral response.
2. Reduce the tile pixels to only the ones that conform to the thresholds in Equation 4. In my experience, these were restrictive enough to reject clouds and bare soil.
3. Use the AOD first-guess $\tau = .2$ and the scene geometry (θ, θ_0, ϕ) to reduce the lookup table and determine aerosol (path) reflectance
4. Subtract the path reflectance from the observed reflectance of any remaining pixels to obtain a surface reflectance estimate. This implies the likely-reasonable assumption that the aerosol attenuation of additional light reflected from the surface is negligible.
5. Check the percentage of pixels with that fit the conditions in Equation 4. If it is greater than 8%, return only the darkest 8% of thresholded pixels in terms of their surface reflectance estimate.
6. If the number of remaining pixels is smaller than 8%, increase the a-priori AOD by $\Delta\tau = .2$, re-calculate surface reflectance, and repeat the process.
7. If the AOD iterates all the way up to $\tau = 3$, reject the tile because the contribution of aerosols should have pushed reflectance beyond the threshold.

4.4 Aerosol Optical Depth Retrieval

Despite the dependence of NIR reflectance on AOD demonstrated by Figure 2, I ultimately decided to determine the “final” estimate for RED channel reflectance in terms of the average reflectance over all DDV pixels in 3 bands in the $.8 - .9 \mu\text{m}$ using the relationship $\text{RED}^* = 0.1 \text{NIR}$, as does (Richter, 2006) [8]. I believe this is an extremely weak assumption, however of all the methods I attempted it was the only one that produced consistent results among multiple granules, and avoids re-using the RED channel reflectances which have already been aggressively constrained by the Equation 4 thresholds and by the iterative DDV pixel selection.

I settled on a 10x10 pixel tile size, so once the DDV selection procedure is complete, each 100-pixel square tile in the field of regard is either rejected, or contains exactly 8 pixels that were identified as dense dark vegetation.

The preliminary step for my AOD retrieval is to reduce the lookup table to the smallest cube of points surrounding the viewing angles, and to use forward-differencing interpolation to determine the effect of an increment change in θ , θ_0 , and ϕ on the TOA observed reflectance (ie $\frac{\partial \rho}{\partial \phi}$) at each AOD bin supported by the lookup table. Since DESIS only has a swath width of 30 km and a FOV of 4.4° , I assume that differences in viewing angles within the field of regard are negligible. As such, the modified lookup table passed to the inversion procedure is merely a 2d array associating optical depth bins with corrected reflectances.

For each valid square, the following procedure is dispatched in order to retrieve a single value for the aerosol optical depth at that tile.

1. Extract the observed reflectance of DDV-masked pixels at $.82\mu\text{m}$, $.85\mu\text{m}$, and $.88\mu\text{m}$, and let NIR^* be the average reflectance between channels and pixels. I assume that this value is representative of the entire tile.
2. Estimate the RED^* surface reflectance such that $\text{RED}^* = 0.1 \text{NIR}^*$.
3. Identify the optical depth bins with reflectances surrounding RED^* and linearly interpolate between them to determine the aerosol optical depth.

5 Results

5.1 Validation Comment

There are 2 ways the DESIS L2 product I used for analysis reports aerosol optical depth. First, the metadata file generated alongside the product has a single value `meanAerosolOpticalThickness` for the entire scene. Alternatively, the quality flags file of the granule contains gridded AOD values, which are scaled to unsigned integer. The DESIS L2 ATBD (Müller, 2015) reports in section 8.6 that the integer encoding corresponds to increments of $\Delta\tau = 0.006$, however in section 8.11 (and in the tiff file) the ATBD suggests that integers are embedded with a scaling factor of $\Delta\tau = 0.01$. As Table 5.2 indicates, of the granules I considered, the 0.01 scaling factor for the quality grid produced values close to the metadata file for only granules G01 and G02. The other 3 granules have acceptable values reported in the metadata for background aerosol content, but quality grid values diverge from the metadata, and seem unreasonably high.

5.2 Analysis

Retrieval	Metric	G01	G02	G03	G04	G05
Mine	Mean	.4936	.5186	.4739	.4241	.4640
	Std Dev	.088	.052	.104	.121	.111
	Min	.003	0.151	0.004	0.006	0.009
	Max	0.598	0.697	0.568	0.583	0.599
Valid	Meta	.2779	.246	.3684	.4755	.3923
	Grid	.2791	.2495	2.270	2.378	2.292

Table 2: Comparison between my retrieval results and AOD values reported in the DESIS metadata, as well as the pixels in the AOD tiff grid corresponding to DDV values.

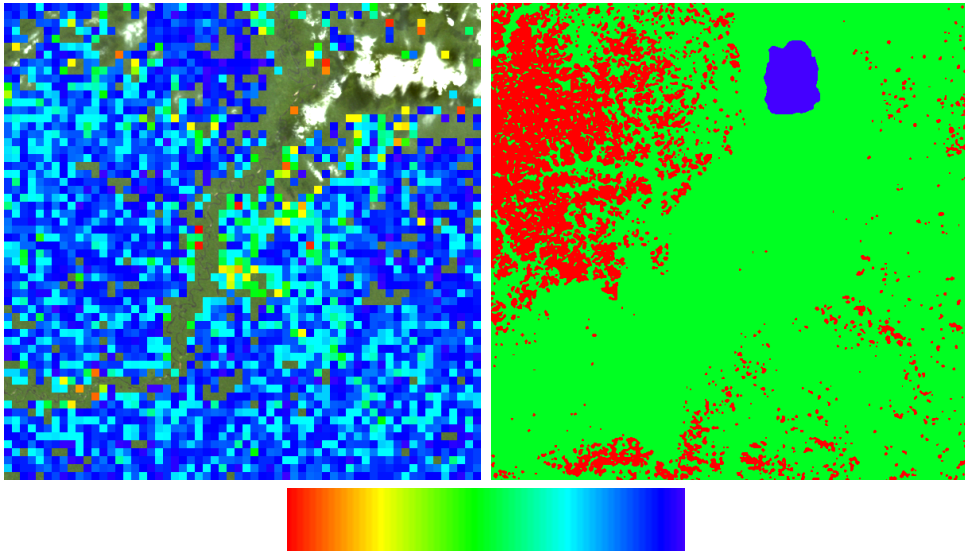


Figure 6: My aerosol optical depth retrieval results for granule G01 (left) versus the DESIS product results (right). This is the same image displayed on the left in Figure 5, and previously characterized with histograms and a spectral response curve. Note that the color bar is deceptive in that the AOD values are independently scaled between their minimum and maximum values. For my retrieval, the color bar represents values in the range $\tau \in [0, .6]$. The aerosol optical depth reported by the file’s metadata represent 3 bins at $\tau = .27$, $\tau = .28$, and $\tau = .29$ with a reported scene average of $\tau = 0.279$.

Table 5.2 and Figures 6 and 7 provide an intercomparison of my AOD values with those included alongside the L2 product. My retrieval values have very low spatial coherence, and generally tend to overestimate the aerosol loading. The lack of consistency isn’t surprising since the margins used to estimate AOD are only a few thousandths of a reflectance factor, and since the standard deviation of the DDV pixels in the near infrared range is still relatively high after thresholding (per Figure 3). I was able to generate retrievals with more even distributions by inverting the lookup table with the thresholded RED reflectances directly, but this seems nonphysical to me because stringent constraints were already artificially placed on the RED reflectance during DDV pixel selection.

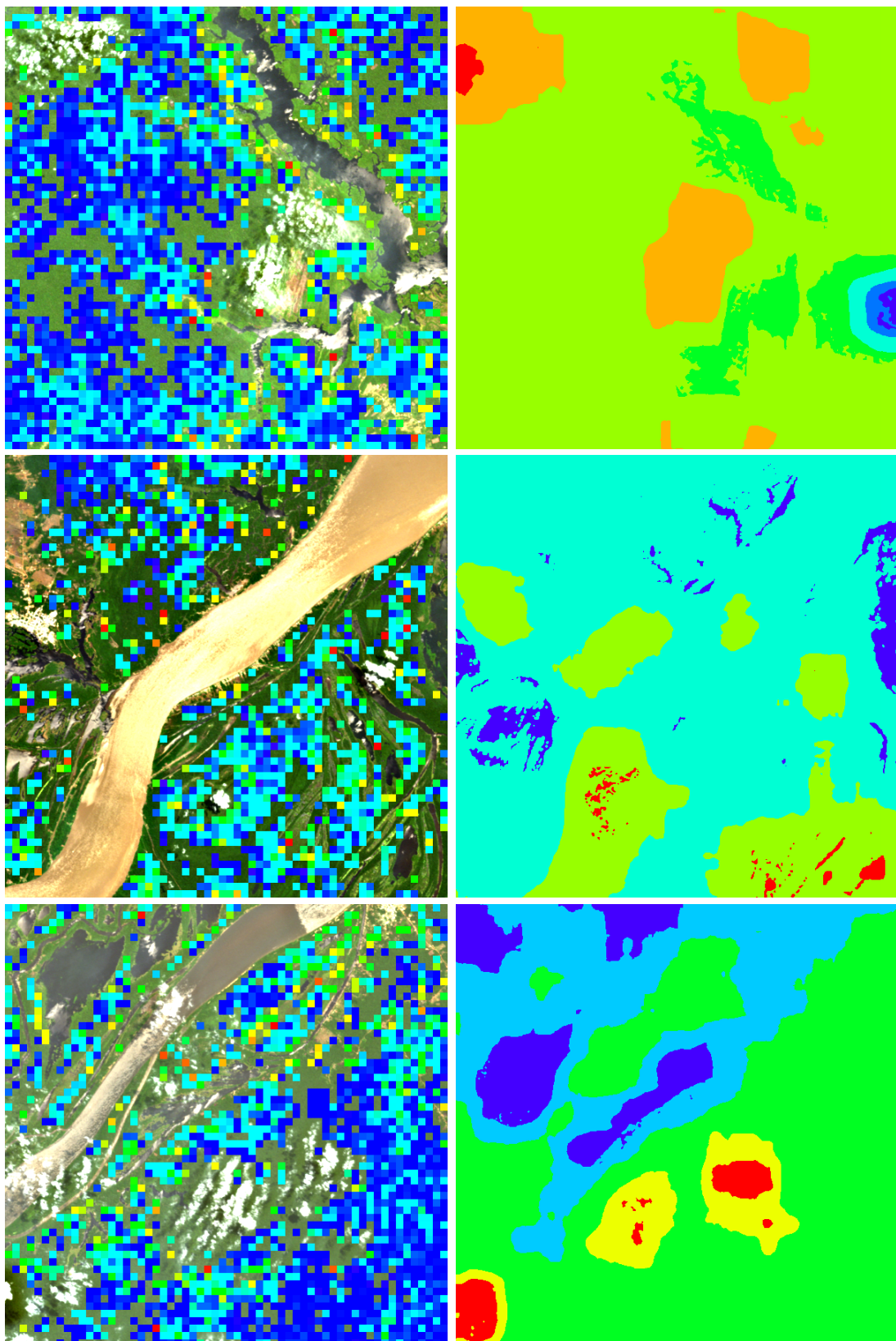


Figure 7: Top: G03; Middle: G04; Bottom: G05. All of the above were captured on 09/03/2020 over the Amazon.

Figure 7 shows several more of the retrievals outlined in Table 5.2. G03 and G05 suggest that the L2 product moves forward with retrievals over regions with substantial cloud shadow and sun glint, which appears to considerably affect the magnitude of their reported values. My retrievals also contain a smattering of anomalously-low AOD values, which seem to mainly correspond to areas where there is likely to be sub-pixel water, and a few regions with cloud shadow.

6 Conclusion

Aerosol optical depth retrievals from satellite radiometers provide information about the composition, spatial distribution, and radiative impact of aerosols on the climate system. Over land, the most common way to characterize aerosols is by using the known relationship between the spectral response of near-infrared and red-band reflectance over dense, dark vegetation. In this project I focused on data with relatively low aerosol loadings over the Amazon. Using the rural continental aerosol model from (Shettle, 1976) [3] and the SBDART radiative transfer model, I generated lookup tables for surface reflectance and TOA spectral radiance with respect to the viewing geometry, wavelengths in $.4 - 1 \mu\text{m}$, and aerosol optical depths between 0 and 20 (modeled at $.55 \mu\text{m}$). With the lookup tables, I followed a procedure similar to [8] to identify 8-pixel groups of the darkest available vegetation in each valid 10x10 tile of pixels throughout the image. Finally, I used the empirical ratio of RED to NIR reflectance to estimate the RED surface reflectance, which is interpolated to an approximate AOD value following a method similar to (Kaufman, 1997) and (Richter, 2006) [6][8].

In all honesty, I'm not convinced that my retrievals provide any physically meaningful information, except perhaps some sense of the relative magnitudes of columnar aerosol attenuation for pixels within a single image. The sensitivity of the RED* surface reflectance estimate to the NIR reflectance makes retrieval values noisy, and the simplistic empirical ratio for estimating their relationship inevitably determines the magnitude of the AOD returned by the inversion. For example, changing the ratio from .1 to .09 caused the mean AOD of my retrievals to decrease by almost half.

References

- [1] D. Tanré, Y. J. Kaufman, M. Herman, and S. Mattoo, “Remote sensing of aerosol properties over oceans using the MODIS/EOS spectral radiances,” *Journal of Geophysical Research: Atmospheres*, vol. 102, no. D14, pp. 16971–16988, 1997. eprint: <https://onlinelibrary.wiley.com/doi/pdf/10.1029/96JD03437>.
- [2] Y. J. Kaufman, D. Tanre, and O. Boucher, “A satellite view of aerosols in the climate system,” *Nature*, vol. 215, 2002.
- [3] E. Shettle and R. Fenn, “Models of the atmospheric aerosols and their optical properties,” *AGARD Conf Proc*, vol. -1, Apr. 1976.
- [4] T. Nakajima and M. Tanaka, “Algorithms for radiative intensity calculations in moderately thick atmospheres using a truncation approximation,” *Journal of Quantitative Spectroscopy and Radiative Transfer*, vol. 40, pp. 51–69, July 1988.
- [5] L. A. Remer, D. Tanré, and Y. J. Kaufman, “MODIS Algorithm Theoretical Basis Document,” 2005.

REFERENCES

- [6] Y. J. Kaufman, D. Tanré, L. A. Remer, E. F. Vermote, A. Chu, and B. N. Holben, “Operational remote sensing of tropospheric aerosol over land from EOS moderate resolution imaging spectroradiometer,” *Journal of Geophysical Research: Atmospheres*, vol. 102, no. D14, pp. 17051–17067, 1997. _eprint: <https://onlinelibrary.wiley.com/doi/pdf/10.1029/96JD03988>.
- [7] R. Richter, “A spatially adaptive fast atmospheric correction algorithm,” *International Journal of Remote Sensing*, vol. 17, pp. 1201–1214, Apr. 1996. Publisher: Taylor & Francis _eprint: <https://doi.org/10.1080/01431169608949077>.
- [8] R. Richter, D. Schläpfer, and A. Müller, “An automatic atmospheric correction algorithm for visible/NIR imagery,” *International Journal of Remote Sensing*, vol. 27, pp. 2077–2085, May 2006. Publisher: Taylor & Francis _eprint: <https://doi.org/10.1080/01431160500486690>.